

Systematic kinetic studies on mixed gas hydrates by Raman spectroscopy and powder X-ray diffraction

Manja Luzi^{a, b, *}, Judith M. Schicks^b, Rudolf Naumann^b and Joerg Erzinger^b

^aIASS Institute for Advanced Sustainability Studies Potsdam
Berliner Straße 130, D-14467 Potsdam
Germany

^bGerman Research Centre for Geosciences GFZ
Telegrafenberg, D-14473 Potsdam
Section 4.2
Germany

* corresponding author. Tel.: +49 331 288 22416; fax: +49 331 288 22404
E-mail address: manja.luzi@iass-potsdam.de (Manja Luzi)

ABSTRACT

This study presents results from systematic time-resolved experiments regarding the guest molecule geometry. The *in situ* observations of formation and dissociation processes of multicomponent hydrates were performed by means of Raman spectroscopy and a newly designed experimental setup including powder X-ray diffraction (PXRD) whose capabilities will be presented here in more detail. Both experimental setups allow investigating hydrate kinetics as a function of pressure, temperature and feed gas composition. The unique feature of both setups is the continuous gas flow providing a constant composition of the gas phase during the whole experiment. This is crucial for the formation of mixed hydrates formed from feed gas mixtures that contain one or more components in low concentrations. The formation of structure II hydrates including C₃H₈, iso-C₄H₁₀, n-C₄H₁₀ or neo-C₅H₁₂ besides CH₄ was analysed according to a multi-step model. For the initial phase it turned out that hydrates grown from the gas mixture containing 2% n-C₄H₁₀ and 98% CH₄ have the highest formation rate at defined p, T conditions in comparison to other hydrates formed from gas mixtures containing about 2 vol% of the above mentioned hydrocarbons besides CH₄. But the reaction mechanisms for each hydrate system emerged to be different. Fur-

thermore, time-resolved Raman and PXRD experiments were performed to study the formation of structure H hydrates with a low-concentrated large hydrocarbon guest molecule. In case of a gas mixture containing 1% iso-C₅H₁₂ and 99% CH₄ the formation of a simple structure I CH₄ hydrate was observed at first. Later on, structure H CH₄ + iso-C₅H₁₂ hydrate was formed resulting in a coexistence of both structures.

Keywords: gas hydrates, kinetics, mixed hydrates, Raman spectroscopy, PXRD

1. Introduction

The knowledge of hydrate formation and dissociation kinetics is pivotal for the gas production from hydrate reservoirs, the selective hydrate formation for the transport of natural gas or for the containment of hydrate plug formation in pipelines. Kinetic data may also be used for numerical simulations regarding the occurrence and composition of natural gas hydrates.

In the past, various kinetic studies on gas hydrate formation and growth processes as well as dissociation processes were performed using a wide range of techniques such as neutron and X-ray diffraction, NMR and Raman spectroscopy. Thereby, hydrate formation processes were mainly studied using ice [1].

The formation of hydrate from ice is a solid-state reaction and therefore takes place at the ice-gas or ice-liquid hydrocarbon interface [2]. In recent years, different models were developed that describe the nucleation and growth process and consider, for instance, the dependency of the formation rate on the surface area of the ice-gas interface [3]. Most of the proposed models have in common that the hydrate formation process proceeds in two to three steps: During the initial stage a hydrate film covers the ice surface. To maintain the hydrate formation either gas molecules or water molecules have to diffuse through the growing hydrate layer. The inward/outward diffusion of gas/water molecules is the rate-limiting second step of the formation process. This mechanism was confirmed by experimental data presented by Takeya et al. [4] and Henning et al. [5]. Henning et al. [5] applied a simple shrinking core model that was originally developed to describe the hydration of cement grains to fit the diffusion-controlled stage. In 2002, Wang et al. [6] extended this model to a third stage, which is controlled by the reaction of the guest molecules with residual ice. However, the authors claim that their model can be reduced to the rate-limiting second stage and modelled the second stage with an approach of Levenspiel [7] that was developed for gas-solid reactions such as tarnishing reactions. Kuhs and co-workers have developed and continuously ed-

ited an own complex mathematical description for the formation of structure I gas hydrates from ice powder based on the finding that some hydrate crystals showed a porous microstructure in the nanoscale [8-13]. From the attempt to treat hydrate formation and decomposition in similar ways Genov [11] suggested a combined Avrami-Erofeev and Ginstling-Brounshtein model. Hydrate formation was again divided into a two-stage process with formation and growth of hydrate nuclei at the beginning modelled by means of the Avrami-Erofeev theory and a diffusion-controlled second stage, which was fitted using the Ginstling-Brounshtein theory.

A similar approach for modelling the formation of structure H hydrates from ice was favoured by Susilo et al. [14]. The authors state that the initial reaction is controlled by intrinsic kinetics and can be therefore fitted with the Avrami equation. The second diffusion-limited stage is described with a simple shrinking-core model based on the Jander equation.

However, the influence of the guest molecules on the kinetics of hydrate formation or dissociation is rarely studied. Recently, it was shown that depending on the formation conditions the chemical nature of the guest molecule (e.g. water solubility) as well as its geometry strongly influence the composition of the hydrate phase. To come close to natural conditions gas mixtures containing small amounts of higher hydrocarbons from C₄ to C₅ were used [15]. Thereby, it turned out that shape and conformation of the guest molecule and hydrate structure cause each other [16].

This work presents a new experimental technique, which allows studying the formation of gas hydrates *in situ*. The goal is to give a first insight into the influence of typical structure II forming hydrocarbons on hydrate formation kinetics based on a three-step hydrate formation model under the aspect of their molecular size and shape. In addition, the same experimental setups were used to study the formation of structure H hydrates from low iso-C₅H₁₂ concentrations.

2. Experimental

Experiments were performed with two different experimental setups, which are both supplied with a continuous gas flow. For instance, one pressure cell is integrated into a setup including a confocal Raman spectrometer (LABRAM, Horiba Jobin Yvon). The Raman sample cell is made from Hastelloy and has a volume of 0.4 cm³. It can be run in a temperature range between 246 K and 353 K and a pressure range between 0.1 MPa and 10 MPa. A thermostat carries out the cooling of the sample cell while the temperature is determined with a Pt 100 temperature sensor with a precision of 0.1 K. The pressure is regulated with an ER 3000 pressure regulator (Tescom Corp.) with a

precision of 2% (rel.). The sample cell is operated with a continuous gas flow of 1 mL/min. Therefore, the incoming gas needs 17 s to pass the cell body before it enters the sample chamber. During this time the incoming gas adjusts to the cell temperature. Furthermore, the pressure cell is equipped with a quartz window. This allows a visual observation of the phases present in the cell as well as the collection of Raman spectra during formation, decomposition or transformation processes of the gas hydrate crystals. For further details regarding the experimental setup the reader is directed to the publication of Schicks et al. [17].

To determine the phase boundary conditions of the mixed hydrates the pressure cell is filled with 150 μ L deionized, degassed water. Next, the sample cell is sealed and flushed with the respective gas mixture before pressurization. Then, the sample cell is cooled down with ca. 2 K/min until a spontaneous crystallization occurs that was mostly observed below 263 K. As indicated from Raman measurements a mixture of ice and hydrate forms at this time. In the next step, the cell is carefully warmed up until at first ice crystals and later on gas hydrate crystals start to dissociate. By the time only a few crystals are left the sample cell is cooled down to ca. 0.5 K below the decomposition limit of the hydrate crystals. At this point, euhedral gas hydrate crystals are allowed to grow. The phase boundary conditions are determined by heating the sample cell slowly until the first crystals start to dissociate.

In order to study formation kinetics the sample cell is filled to one third with powdered ice. Therefore, ice was generated from deionised water that was frozen in a liquid nitrogen bath. Afterwards the ice was powdered in a 6750 freezer mill (Spex CertiPrep) that was also cooled with liquid nitrogen. By means of scanning electron microscopy the diameter of these ice particles was accounted to be in between 10 to 20 μ m. Figure 1 shows a SEM image of freshly prepared ice powder. As the ice particles are exposed to ambient air frost may form on their surface. Once filled into the pressure cell the ice was kept until it attained the cell temperature of 271 K. Afterwards, the sample cell was pressurized and data acquisition was started.

Time-dependent PXRD measurements were performed with a low-temperature-high-pressure cell that was integrated into a Bruker AXS Discover diffractometer. The concept of this experimental setup is similar to the pressure cell, which is combined with the Raman spectrometer that was described before. The pressure cell is made from stainless steel with a hole of 0.5 cm diameter in its centre and has a volume of 250 μ L. Both sides of the cell body are sealed with beryllium plates and tightened with O-rings. The cell can be operated in a pressure range between 0.1 to 4.0 MPa.

The pressure is also regulated with an ER 3000 pressure regulator. The temperature is controlled by means of a Peltier-cooling device (Kryotherm model TB-119-1.4-1.15CH) that also contains a hole of 0.5 cm. The Peltier-cooling provides quick temperature changes and a precise temperature control of ± 1.0 K by use of an adjustable power source and a controlling device (West 4200, West Instruments Ltd). The cell can be run in a temperature range between 253 K and 288 K. The cell was designed for the use in combination with a Bruker AXS D8 Discover microdiffractometer with Cu-K α -radiation generated at 40 kV and 40 mA. The diffractometer has parallel beam optics (Goebel mirror) to optimize the beam intensity that enables the analysis of powder samples with a non-planar surface. A mono-capillary, which narrows the beam to a diameter of 300 μm , was applied. In consequence, small sample areas and consequently small sample amounts of gas hydrate powder can be investigated in the micrometer range. The detection of the diffracted X-rays is carried out with GADDS (General Area Detection Diffraction System), which includes a High Star area detector. A more detailed description of the experimental setup can be found by Luzi et al. [18]. For a typical kinetic experiment the precooled sample cell is filled with approximately 100 μL powdered ice, carefully sealed and mounted on the XYZ stage of the diffractometer. Thereby, the ice sticks on the beryllium window, which is situated on the side of the Peltier cooling device. Next, the sample cell is pressurized with the respective gas mixture and the data acquisition is commenced and lasts for at least 8 h. The frequency of data collection depends on the transformation rate of ice into hydrate. Due to the narrow beam various positions within the sample can be measured in a short sequence. Commonly, five defined measuring points, which are randomly distributed within the sample cell, are chosen for analysis. A list of the gas mixtures used in this study is given in table 1.

3. Results and discussion

3.1 Guest molecule diameter

Although the large hydrocarbon guest molecules used in this study are known structure II formers their ability to fill the hydrate cage in a proper way is different and depends to a great extent on the molecular shape and diameter [1]. The van der Waals diameter of the guest molecules was calculated by summation of the molecular diameter, which was determined using the software CS Chem3D Pro Version 7.0 from Cambridge Soft, and the van der Waals radius of the outer hydro-

gen atoms. The utilized van der Waals radius of the hydrogen atoms is 110 pm and was obtained from Mantina et al. [19]. This procedure is obeyed as an approximation. Table 2 provides an overview of the van der Waals diameters of the large hydrocarbon guest molecules. As is known $n\text{-C}_4\text{H}_{10}$ has more than one conformation. The respective van der Waals diameters of the three conformers are also given in table 2. Effectively, the trans conformer would be too large to fit into the $5^{12}6^4$ cavity of structure II [1]. But as n -butane was verified as structure II former the shape of the molecule must also play a certain role. From dielectric [20] and Raman measurements [21] and recently single crystal X-ray diffraction [16] it was shown that n -butane is incorporated into the hydrate cage as its gauche conformer.

3.2 Phase equilibria data

Time-dependent PXRD experiments were performed at defined p, T conditions within the stability field of the mixed hydrates. In order to evaluate the influence of the large hydrocarbon guest molecule the experiments were conducted at the same temperature (267 K) and 75% above the equilibrium pressure regarding each gas mixture. Therefore, the phase boundaries for the mixed hydrates had to be determined both experimentally and by means of the software CSMGem [22]. Figure 2 shows the phase diagram for the mixed hydrates containing C_3H_8 , $\text{iso-C}_4\text{H}_{10}$, $n\text{-C}_4\text{H}_{10}$ or $\text{neo-C}_5\text{H}_{12}$ besides CH_4 . The experimental data (displayed as squares) are compared with modelled data (displayed as lines), which were determined by means of CSMGem [22]. Apparently, experimental and modelled data show a good agreement. Hydrate phase equilibria were not only modelled for the liquid water-hydrate-vapour ($\text{L}_\text{W}\text{-H-V}$) region but also for the ice-hydrate-vapour (I-H-V) region because these data were required for the kinetic experiments. $\text{CH}_4 + \text{neo-C}_5\text{H}_{12}$ hydrate is the only system whose phase equilibria could not be modelled with CSMGem because the guest molecule $\text{neo-C}_5\text{H}_{12}$ is not integrated in the program. Therefore, the decomposition line was derived from an exponential fit ($R^2 > 0.99$) of the experimental data obtained in the $\text{L}_\text{W}\text{-H-V}$ region and extended into the I-H-V region. Obviously, this is a mistake because the change of the slope of the decomposition line at the quadruple point (approximately at 273 K) where the four phases ($\text{I-L}_\text{W}\text{-H-V}$) coexist is not obeyed. However, in terms of absolute values the mistake is supposed to be rather low because the equilibrium pressure for $\text{CH}_4 + \text{neo-C}_5\text{H}_{12}$ hydrate at 273 K is ca. 0.6 MPa.

Table 3 shows the p, T conditions for the time-dependent PXRD experiments. The measurements were conducted at the same temperature and a (composition-related) pressure of 75% above the respective equilibrium pressure.

3.3 Analysis of time-dependent PXRD data

Figure 3 presents the results of a time-resolved PXRD experiment showing the conversion of hexagonal ice into a cubic structure II hydrate that was formed from gas mixture GM_nC4. The hydrate was grown at 2.36 MPa and 267 K. The transformation process is shown for one out of five measuring points. The prominent diffraction peaks from the ice and the hydrate phase are labelled by the Miller indices of the respective crystal planes. At the beginning of the experiment only the four ice reflections occur (see figure 3 at $t = 0$ min). After 8 min hydrate crystal formation starts which is expressed with the occurrence of the hydrate reflections. In the course of the experiment the hydrate reflections increase while the intensities of the ice reflections decrease. This leads to the conclusion that the ice phase is converted into a structure II gas hydrate. The integrated intensity of a reflection is proportional to the crystal volume. A change of the integrated intensity is therefore associated with a volume change of the hydrate or ice phase. The rate of change provides information about formation, dissociation or transformation rates of the hydrate crystals [4].

Unfortunately, the diffraction data could not be quantified by the typically used Rietveld refinement method. Therefore, the diffraction data were analysed in a semi-quantitative way that included a single line analysis. In order to estimate the progress of the transformation process between the two crystal structures a representative reflection for each phase was chosen. In case of hexagonal ice the reflection for the (100) crystal plane at circa $22.8^\circ 2\theta$ was used, and for structure II the reflection for the (531) crystal plane at circa $30.3^\circ 2\theta$ was used. This reflection was chosen because it does not overlap with reflections from the ice phase. From both values the relative intensity ratio between the hydrate phase and the ice phase was calculated, which is considered as total reaction constant α . The calculation of the peak areas is done by means of the Bruker AXS TOPAS program. As data from five measuring points are obtained a mean value for the intensity ratio can be determined. The error is the standard deviation. Figure 4 shows the total reaction extent α (resulting from the semi-quantitative analysis) for the formation of $\text{CH}_4 + \text{n-C}_4\text{H}_{10}$ hydrate starting from a pure ice phase for the first 8 h.

3.4 Description of the hydrate formation model

Based on the above described literature findings the hydrate formation process from ice was divided into three stages. During the first step hydrate crystals start to nucleate and grow on the surface of an ice particle. The incipient hydrate growth occurs on various active sites on the surface resulting in a thin hydrate film that spreads around the ice particle. At this time the formation rate is supposed to be basically limited by the enclathration reaction. Once a hydrate film has formed the growth rate is assumed to be mainly controlled by the inward diffusion of the gas molecules through the hydrate layer to the unreacted ice core or the outward transport of water molecules to the hydrate-gas interface. But the appearance of ice imperfections such as lattice defects, cracks and pores may influence the start and the progress of the second step distinctly [12, 23]. At conversion rates above 90% a third step was observed. At this point, the hydrate formation rate slows down markedly and seems to be no longer controlled by diffusion but by the reaction of depleting unreacted ice particles with the gas molecules. Naturally, this step of hydrate formation was observed for only a low number of systems and also incompletely. Therefore, a mathematical description of this process is not done.

The initial hydrate formation step controlled by the enclathration reaction is modelled using the Avrami rate law. Lots of solid-state reactions such as crystalline growth can be described by relations that are based on the process of nucleation. Random nucleation followed by the growth of the nuclei is often modelled using the Avrami rate law (also known as Avrami-Erofeev or Johnson-Mehl-Avrami-Kolmogorow equation) [23, 24]. This equation has been successfully used before to fit data from hydrate formation experiments [2, 11, 14]. The reaction extent α can be given by a general expression of the Avrami rate law being

$$\alpha = 1 - \exp(-kt^n), \quad (1)$$

whereby k is the formation rate constant, n is the Avrami exponent and t is the time. Taking twice the logarithm of equation 1 results in the following form

$$\ln(-\ln(1 - \alpha)) = \ln k + n \ln t. \quad (2)$$

The triple logarithmic plot should give a straight line whose slope refers to n and the intercept corresponds to $\ln k$. Typically, reactions following the Avrami rate law exhibit a sigmoid growth function. The shape of the graph is dependent on the values of n . If the formation of nuclei is rapidly finished after the beginning of the transformation process and no further nucleation occurs (site saturated nucleation), the value of the Avrami exponent can be directly related to the dimension of the growth. Thereby, the growth of spherical nuclei in three dimensions equals to $n = 3$, the two-dimensional or plate-like growth corresponds to $n = 2$ and the one-dimensional or lineal growth is consistent with $n = 1$. If nucleation occurs throughout the whole transformation process with a constant rate, the Avrami exponent becomes equal to $n + 1$, e.g. 4 for three-dimensional growth, 3 for two-dimensional growth and so on. But the Avrami exponent can also take on values below one, which most likely results from decreasing nucleation and growth rates [25]. In case of mass transfer resistance like diffusion decisively affects the growth rate, the Avrami exponent is reduced by a factor of two and subsequently may take on value below one [25, 26].

The second step of the conversion of an ice particle into hydrate is supposedly controlled by diffusion. Once a hydrate layer has formed either gas molecules or water molecules have to diffuse through this layer to continue the enclathration reaction. Levenspiel presented a general model where diffusion of a reactant through a continuously growing product layer controls the rate of reaction [7]. Basically, a substance A diffuses through the product layer AB and reaches the reaction zone i.e. the surface of substance B. Thereby, substance A and the boundary of the unreacted material B move towards the centre of the spherical particle. Equation 3 shows the diffusion-controlled rate of a reaction as it was derived from Levenspiel.

$$kt = 1 - 3(1 - \alpha)^{2/3} + 2(1 - \alpha), \quad (3)$$

where k is again the formation rate constant, t is time and α is the total reaction extent. Plotting t against the term $1 - 3(1 - \alpha)^{2/3} + 2(1 - \alpha)$ the rate constant k can be obtained from the slope of the curve.

Apparently, neither the Avrami nor the Levenspiel model was originally developed to analyse hydrate formation kinetics. Therefore, these models have to be used with caution. A recent publication of Falenty et al. [27] for instance mentions that for micrometer-sized ice particles (also referred to as frost) the initial hydrate film does not form because this already exceeds the ice particle dimensions. The authors argue that in this case “the ice grains are directly consumed by a

growing nucleus created on the particle surface”. For this reason the Avrami equation cannot be applied to the hydrate formation from micrometer-sized ice particles (particle size of 2.5-7.5 μm) because the Avrami model assumes “...an infinitively large domain of crystallization” [27]. Noteworthy, this effect is not supposed to have an essential impact on the results presented here because the ice particles used in this work have an average diameter of ca. 10-20 μm although they are also partly covered with frost.

3.5 Results of kinetic analysis

The data obtained from *in situ* PXRD experiments were analysed according to equation 1 and 3. For the experiments presented here, the third step in the transformation process from ice into structure II hydrate was not observed. Hydrate formation reactions were usually observed for at least 8 h to enable the identification of single reaction stages. Figure 5 shows a two-step analysis of the formation process of $\text{CH}_4 + \text{C}_3\text{H}_8$ hydrate. Figure 5a, 5b and 5c include the experimental data for the hydrate formation reaction recorded for 500 min at 1.26 MPa and 267 K, the respective triple logarithmic plot for the overall reaction and the plot for the diffusion-controlled second step for one out of five measuring points.

In order to find out if and at what point the reaction changes from initial nucleation and growth to diffusion control the complete data set for the $\text{CH}_4 + \text{C}_3\text{H}_8$ hydrate was displayed in the triple logarithmic plot. From figure 5b it comes out that the Avrami fit works within the first 40 min ($\ln t = 3.76$) of hydrate formation. After 40 min the curve shows a turning, which indicates a change of the reaction mechanism. The subsequent hydrate formation is most likely dominated by a diffusion-controlled reaction and is therefore analysed by means of the Levenspiel equation. To meet the conditions of equation 3 the amount of hydrate formed during the first step was deducted and the corrected reaction time t^* was introduced starting with $t^* = 0$. So, α^* is the total reaction extent when diffusion overtakes the control of the reaction rate. From figure 5c it becomes apparent that the fitting related to diffusion control is successful. A two-step analysis could also be carried out for the $\text{CH}_4 + \text{neo-C}_5\text{H}_{12}$ hydrate.

In contrast to the previous example, it is also possible that a hydrate formation reaction is only weakly influenced by diffusion. Figure 6 shows the hydrate formation reaction for $\text{CH}_4 + \text{n-C}_4\text{H}_{10}$ that was observed for 480 min and the triple logarithmic plot for the complete reaction.

From figure 6a it becomes obvious that the amount of hydrate reaches ca. 65% (rel.) within the observed time period. Remarkably, the Avrami fit (figure 6b) succeeds for the complete period that was recorded. This indicates that the formation rate is governed by the enclathration reaction and it is furthermore not controlled but presumably only slightly affected by diffusion within this time. The same effect was also observed for the CH₄ + iso-C₄H₁₀ hydrate. Table 4 and 5 give an overview on the formation rate constants that were obtained for the reaction-controlled formation steps and diffusion-controlled steps, respectively.

Regarding table 4 and 5 two different tendencies can be observed. First, for the mixed hydrates containing C₃H₈ and neo-C₅H₁₂, respectively, a two step-process can be applied. This implies that after an initial nucleation reaction diffusion determines the formation rate constant. Secondly, for the mixed hydrates that contain n-C₄H₁₀ and iso-C₄H₁₀ the observed part of the formation reaction can be completely described by means of the Avrami model.

In terms of absolute values CH₄ + n-C₄H₁₀ hydrate shows the highest formation rate constant for the enclathration-controlled reaction as comes out from table 4. It is followed by the mixed hydrates including C₃H₈ and iso-C₄H₁₀, which are in the same order of magnitude. The k value of CH₄ + neo-C₅H₁₂ hydrate is two order magnitudes less. In regard of the pressure-temperature diagram (figure 2) and the molecular diameters (table 2) this result is rather surprising. Starting from the same temperature the CH₄ + n-C₄H₁₀ hydrate shows the highest equilibrium pressure compared to other mixed hydrates also because n-C₄H₁₀ does not ideally fill the large cage of structure II [16]. In terms of molecular diameter C₃H₈, iso-C₄H₁₂ and neo-C₅H₁₂ have similar values and show a more favourable size to cavity ratio [1]. Therefore, the molecular size and shape does not seem to be related to the hydrate formation rate at least during the first step.

In case of neo-C₅H₁₂ it was pointed out before that the p, T conditions applied during the PXRD experiments are based on own experimental data that were obtained in the L_W-H-V region. Flowingly, the calculation of p, T values below 273 K from the experimental data might be imperfect resulting in too low p values. Consequently, the formation rate constants for CH₄ + neo-C₅H₁₂ might be underestimated.

In addition to k values the Avrami model also delivers indications regarding the dimension of the crystal growth. Assuming that the nucleation occurs instantaneously when the cell is pressurized a value of $n = 1$ can be expected which corresponds to a one-dimensional growth in the form of dendrites or needles. However, the Avrami exponents for the hydrates containing the C₃H₈, iso-C₄H₁₀ and n-C₄H₁₀ are less than one. An n value below one indicates that the nucleation and

growth rate are decreasing during the formation process due to decreasing nucleation and growth sites. Since the particle size distribution for the ice particles is not homogenous and the ice particles are presumably also covered with frost it seems to be reasonable that the smaller particles react first and convert also faster into hydrate. As a result the number of possible nucleation sites and also the growth rate decreases. However, it is not clear to what extent mass transfer effects affect the formation rates. For $\text{CH}_4 + \text{neo-C}_5\text{H}_{12}$ hydrate the value for the Avrami exponent is $n = 1.71$, which indicates a 1D/2D dimensional growth of hydrate crystals.

Contrary to the binary hydrates including iso- C_4H_{10} or n- C_4H_{10} , for $\text{CH}_4 + \text{C}_3\text{H}_8$ hydrate and $\text{CH}_4 + \text{neo-C}_5\text{H}_{12}$ hydrate the initial nucleation and growth process is followed by a change of the reaction mechanism where the formation rate slows down. The second step can be successfully fitted by means of the diffusion-controlled model. Compared to C_3H_8 , the molecular diameter of neo- C_5H_{12} is slightly larger which also influences the rate of diffusion. From table 5 it comes out that the k value for $\text{CH}_4 + \text{neo-C}_5\text{H}_{12}$ hydrate is smaller which supports this assumption.

From the gained parameters it might be concluded that the mixed hydrates containing n- C_4H_{10} and iso- C_4H_{10} show a fast instantaneous nucleation which is presumably immediately accompanied by mass transfer effects as there is no change of mechanism observable from the triple logarithmic plot. In contrast, the $\text{CH}_4 + \text{C}_3\text{H}_8$ and $\text{CH}_4 + \text{neo-C}_5\text{H}_{12}$ hydrates exhibit a two-step mechanism including an initial hydrate nucleation and growth stage followed by a diffusion-controlled stage.

The reasons for this behaviour seem to be rather complex and do not only depend on the molecular size and shape in the first order. At least, the presented results are tentative and need more discussion.

3.6 In situ Raman and PXRD analysis of $\text{CH}_4 + \text{iso-C}_5\text{H}_{12}$ hydrate formation

Time-dependent measurements employing Raman spectroscopy and PXRD were also conducted with a gas mixture consisting of 1% iso- C_5H_{12} and 99% CH_4 . Figure 7 shows PXRD diagrams as a function of time collected during $\text{CH}_4 + \text{iso-C}_5\text{H}_{12}$ hydrate formation from ice at one measuring point at 267 K and 1.06 MPa. Please note, that the chosen p, T conditions are located within the stability fields of structure I CH_4 hydrate as well as structure H $\text{CH}_4 + \text{iso-C}_5\text{H}_{12}$ hydrate which was estimated using CSMGem [22].

The experiment starts from hexagonal ice, which is labelled in figure 7. Remarkably, after 7 min the first reflections that occur from a new phase arise from cubic structure I. After ca. 120 min a

small shoulder starts to form at $18.3^\circ 2\theta$ that was not recorded for pure cubic structure I hydrates in reference experiments before. The hydrate formation was observed for more than 12 h. Analysis of the position of the diffraction peaks showed that the formation of a cubic structure I hydrate is followed by the formation of a hexagonal structure H hydrate. The whole experiment was run for 48 h under the same conditions showing a decreasing amount of ice but a continuous coexisting of structure I and structure H hydrate crystals.

To analyse the composition of the coexisting hydrate phases the experiment was repeated with the experimental setup that includes the Raman spectrometer. Figure 8 shows a photograph taken from the obtained hydrate phase. The confocal Raman setup allows the analysis of defined spots within the sample which are marked with a and b in figure 8. Figure 9 presents the respective Raman spectra.

For the Raman spectra shown in figure 9 the region of the C-H vibrational frequencies of hydrocarbons was chosen. Figure 9a displays the typical split signal for the ν_1 C-H symmetric stretching vibration of methane trapped in the small (5^{12}) and in the large ($5^{12}6^2$) cage of structure I [1]. The determination of the relative band intensities shows an intensity ratio of 3:1. Apparently, the Raman spectrum (figure 9b) of the nearby crystal b) shows additional vibrational frequencies that were assigned to iso-C₅H₁₂ and are marked by an asterisk [28]. Furthermore, the Raman bands at 2915 cm^{-1} and 2905 cm^{-1} presumably arise from CH₄ in small (5^{12}) and in the medium ($4^35^66^3$) cages of structure H [1]. Consequently, the Raman experiment confirms the findings from the PXRD experiment i.e. the formation of coexisting structure I and structure H hydrate crystals from a gas mixture containing CH₄ and a structure H hydrate former in low concentrations. Although iso-C₅H₁₂ is continuously supplied due to the gas flow system the concentration is not sufficient to generate a single structure H hydrate phase, only. Noteworthy, for a hydrate grown from CH₄ and liquid iso-C₅H₁₂ (with 200% of the necessary stoichiometric amount of iso-C₅H₁₂ needed to form structure H) only structure H hydrate was found [16]. At the here chosen experimental conditions structure I CH₄ hydrate is preferentially formed followed by the formation of a structure H CH₄ + iso-C₅H₁₂ hydrate, which was observed from Raman and PXRD. Thus, our results from *in situ* experiments confirm the recent findings of Yeon et al. [29] who demonstrated the coexistence of structure I and structure H hydrate crystals in a bulk hydrate phase grown from 2.8% iso-C₅H₁₂ and 97.2% CH₄ by means ¹³C NMR and Raman spectroscopy.

4. Summary and conclusions

The main goal of this study was to present a new *in situ* technique to investigate hydrate formation kinetics and to give a first insight into the influence of the guest molecule size on the hydrate formation rate. Therefore, mixed structure II hydrates containing C₃H₈, iso-C₄H₁₀, n-C₄H₁₀ or neo-C₅H₁₂ besides CH₄ were grown at comparable conditions that were figured out before from experimental and modelled phase equilibria data. Hydrate formation was followed by *in situ* PXRD and analysed by means of a three-step model whereby the third stage was not observed for these experiments. The first stage including the initial formation and growth of a hydrate layer was modelled with the Avrami equation. The Levenspiel model for diffusion-controlled reactions is used to describe the second stage. It turned out that the mixed hydrates follow two different reaction mechanisms. The formation of the hydrates containing iso-C₄H₁₀ and n-C₄H₁₀, respectively, can be completely described with the Avrami model. The formation rate constants for the observed period are determined by the enclathration reaction. The hydrates grown from the gas mixtures containing C₃H₈ and neo-C₅H₁₂ show a change in the formation mechanism, which allowed the application of a typical two-step formation model. Regarding the guest molecule size and shape, this does not seem to influence the formation rate at least during the enclathration-controlled stage of hydrate formation. Remarkably, the n-C₄H₁₀ containing hydrate has the highest formation rate although its size to cavity ratio is much less favourable as it is for the other large hydrocarbon guest molecules examined here. In contrast, for the diffusion controlled second step the guest molecule with the smaller molecular diameter shows the larger reaction rate.

However, from the here presented *in situ* PXRD experiments of the binary structure II hydrates it remains unclear what caused the observed change of the reaction mechanism. Except from guest composition and absolute pressure all parameters were kept constant. So, the reason is assumed to be related to one of these parameters. Therefore, further experiments with varying pressure are performed whose results will be presented later.

In addition, the formation reaction of hydrates grown from CH₄ and a low concentrated structure H former was studied using Raman spectroscopy and PXRD. From both experiments it was observed that a structure I CH₄ hydrate forms in the first place. Thereupon, an iso-C₅H₁₂ containing structure H hydrates forms in coexistence with the structure I CH₄ hydrate.

Acknowledgements

The authors thank the staff of the GFZ workshops for the invaluable technical help and for the construction of the pressure cells.

References

- [1] E.D. Sloan, C.A. Koh, Clathrate Hydrates of Natural Gases, third ed., CRC Press, Boca Raton, 2008.
- [2] I.L. Moudrakovski, A.A. Sanchez, C.I. Ratcliffe, J.A. Ripmeester, *J. Phys. Chem. B* 105 (2001) 12338-12347.
- [3] R.M. Barrer, A.V.J. Edge, *Proceedings of the Royal Society of London. Series A. Mathematical and Physical Sciences* 300 (1967) 1-24.
- [4] S. Takeya, T. Hondoh, T. Uchida, *Ann NY Acad Sci* 912 (2000) 973-982.
- [5] R.W. Henning, A.J. Schultz, V. Thieu, Y. Halpern, *J. Phys. Chem. A* 104 (2000) 5066-5071.
- [6] X. Wang, A.J. Schultz, Y. Halpern, *J. Phys. Chem. A* 106 (2002) 7304-7309.
- [7] O. Levenspiel, *Chemical Reaction Engineering*, John Wiley & Sons, New York, 1999.
- [8] A.N. Salamatin, W.F. Kuhs, in: *Proceedings of the Forth International Conference on Gas Hydrates*, Yokohama, 2002.
- [9] D.K. Staykova, W.F. Kuhs, A.N. Salamatin, T. Hansen, *J. Phys. Chem. B* 107 (2003) 10299-10311.
- [10] G. Genov, W.F. Kuhs, D.K. Staykova, E. Goreschnik, A.N. Salamatin, *Amer. Mineral.* 89 (2004) 1228–1239.
- [11] G. Genov, *Physical processes of the CO₂ hydrate formation and decomposition at conditions relevant to Mars*, PhD thesis, Georg August Universität, Göttingen, 2005.
- [12] W.F. Kuhs, D.K. Staykova, A.N. Salamatin, *J. Phys. Chem. B* 110 (2006) 13283-13295.
- [13] A. Falenty, *Formation and decomposition processes of CO₂ hydrates at conditions relevant to Mars*, PhD thesis, Georg-August-Universität, Göttingen, 2008.
- [14] R. Susilo, J.A. Ripmeester, P. Englezos, *AIChE Journal* 53 (2007) 2451-2460.
- [15] J.M. Schicks, M. Luzi, J. Erzinger, E. Spangenberg, in: W.F. Kuhs (Ed.), *Physics and Chemistry of Ice*, RSC Publishing. Cambridge, 2007, pp. 537-544.

- [16] M. Luzi, J.M. Schicks, R. Naumann, J. Erzinger, K. Udachin, I. Moudrakovski, J.A. Ripmeester, R. Ludwig, in: Proceedings of the 6th International Conference on Gas Hydrates, Vancouver, 2008.
- [17] J.M. Schicks, R. Naumann, J. Erzinger, K.C. Hester, C.A. Koh, E.D. Sloan, *J. Phys. Chem. B* 110 (2006) 11468-11474.
- [18] M. Luzi, M. Girod, R. Naumann, J.M. Schicks, J. Erzinger, *Rev. Sci. Instrum.* 81 (2010) 125105.
- [19] M. Mantina, A.C. Chamberlin, R. Valero, C.J. Cramer, D.G. Truhlar, *J. Phys. Chem. A* 113 (2009) 5806-5812.
- [20] D.W. Davidson, S.K. Garg, S.R. Gough, R.E. Hawkins, J.A. Ripmeester, *Can. J. Chem.* 55 (1977) 3641-3650.
- [21] S. Subramanian, E.D. Sloan, *J. Phys. Chem. B* 106 (2002) 4348-4355.
- [22] A.L. Ballard, E.D. Sloan, *Fluid Phase Equilib.* 194-197 (2002) 371-383.
- [23] J.E. House, *Principles of Chemical Kinetics*, Elsevier, San Diego, 2007.
- [24] M. Fanfoni, M. Tomellini, *Il Nuovo Cimento D* 20 (1998) 1171-1182.
- [25] T. Pradell, D. Crespo, N. Clavaguera, M.T. Clavaguera-Mora, *J. Phys.: Condens. Matter* 10 (1998) 3833-3844.
- [26] U.W. Gedde, *Polymer Physics: Crystallization Kinetics*, Chapman and Hall, London, 1995.
- [27] A. Falenty, G. Genov, T.C. Hansen, W.F. Kuhs, A.N. Salamatina, *J. Phys. Chem. C* 115 (2011) 4022-4032.
- [28] N.G. Mirkin, S. Krimm, *J. Mol. Struct.* 550-551 (2000) 67-91.
- [29] S.-H. Yeon, J. Seol, H. Lee, *JACS* 128 (2006) 12388-12389.

Figures:

FIGURE 1. SEM image of freshly prepared ice powder.

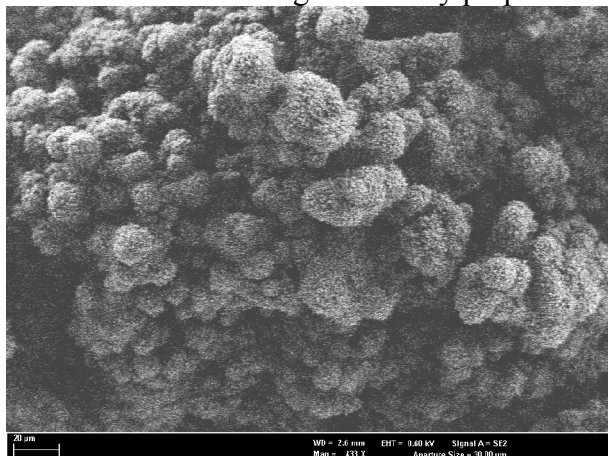


FIGURE 2: Phase diagram of mixed gas hydrates including experimental and modelled data: ▲, 2% n-C₄H₁₀ 98% CH₄; ■, 2% C₃H₈ 98% CH₄; ●, 2% iso-C₄H₁₀ 98% CH₄; ★, 2% neo-C₅H₁₂ 98% CH₄; —, modelled values using CSMGem or exponential fit for neo-C₅H₁₂ + CH₄ hydrate.

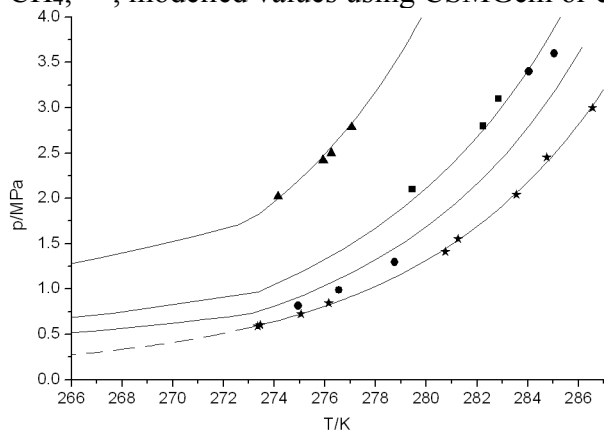


FIGURE 3. Time-resolved PXRD diagrams showing the growth of CH₄ + n-C₄H₁₀ hydrate at 267 K and 2.36 MPa.

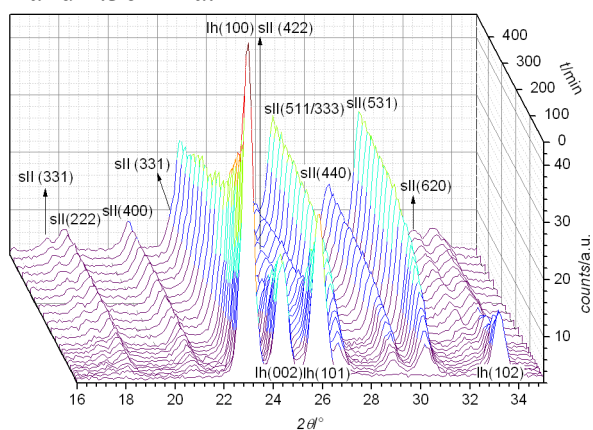


FIGURE 4. Mean formation rate of $\text{CH}_4 + n\text{-C}_4\text{H}_{10}$ hydrate at 267 K and 2.36 MPa.

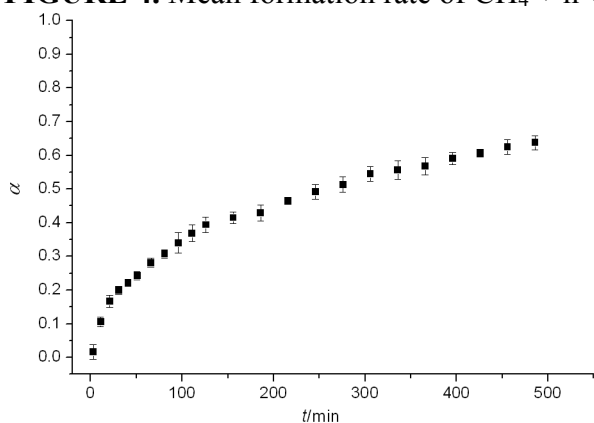
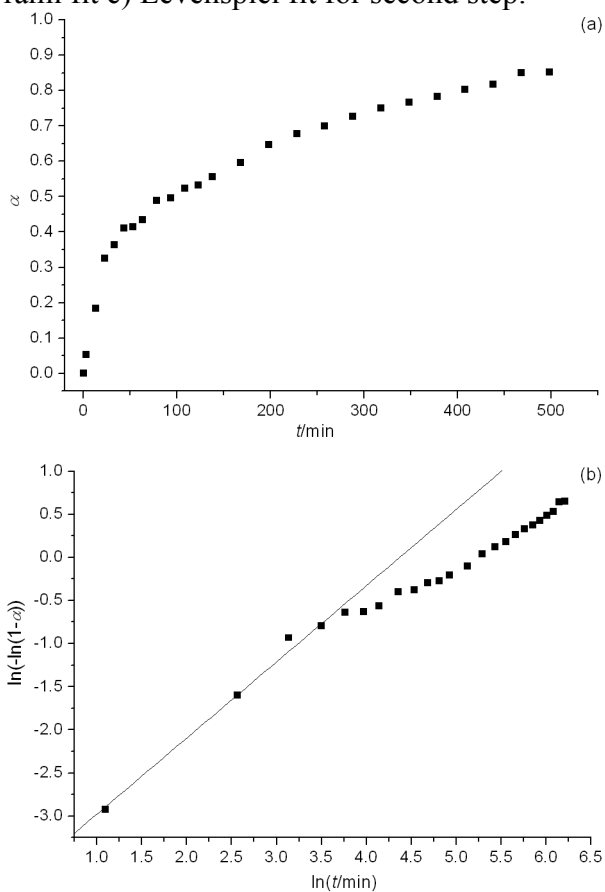


FIGURE 5. a) Formation reaction of $\text{CH}_4 + \text{C}_3\text{H}_8$ hydrate for one measuring point b) overall Avrami fit c) Levenspiel fit for second step.



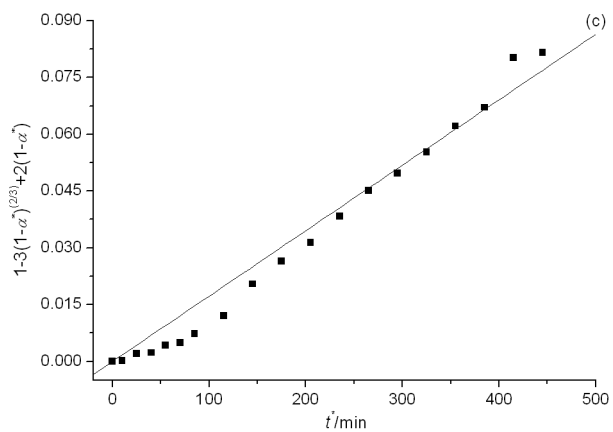


FIGURE 6. a) Formation reaction of CH₄ + n-C₄H₁₀ hydrate for one measuring point b) overall Avrami fit.

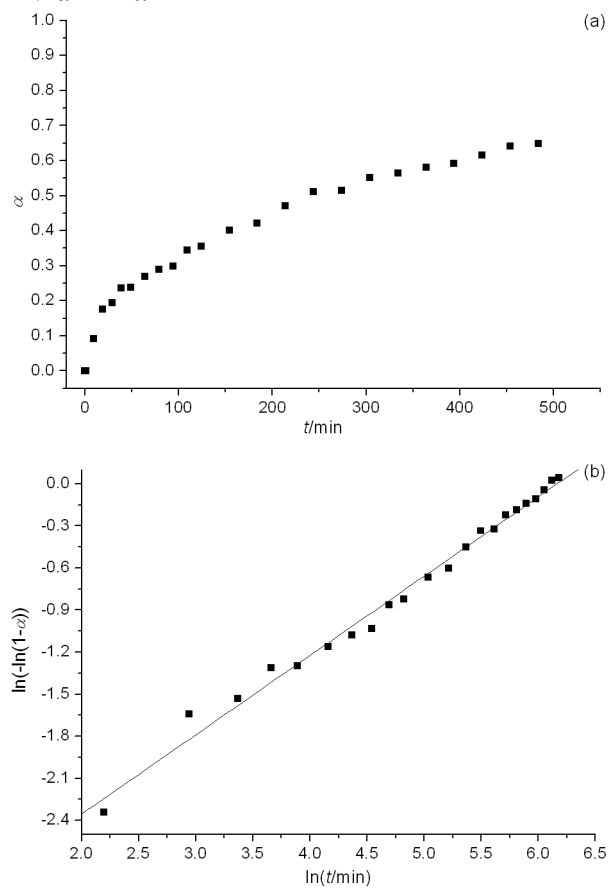


FIGURE 7. Time-resolved PXRD diagrams showing the formation of structure I and structure H gas hydrates from ice.

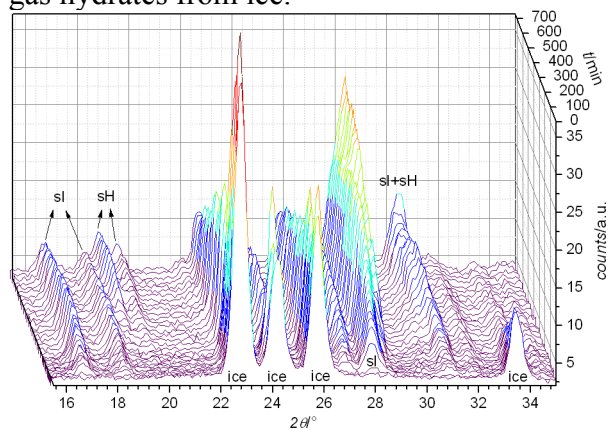


FIGURE 8. Photograph of hydrate crystals grown from a gas mixture containing 1% iso-C₅H₁₂ and 99% CH₄.

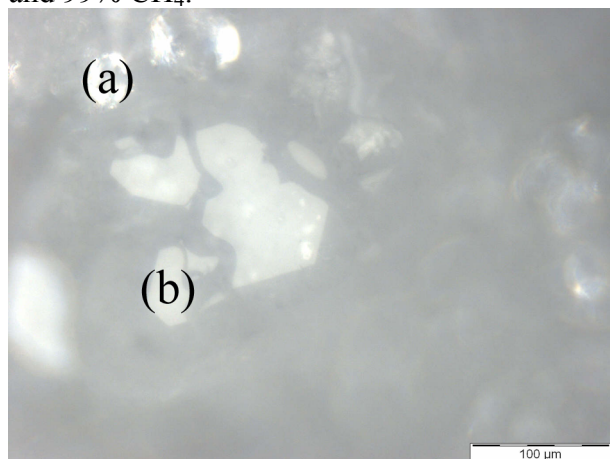
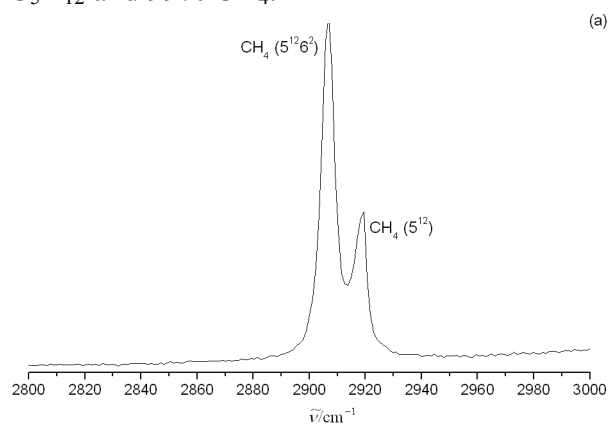
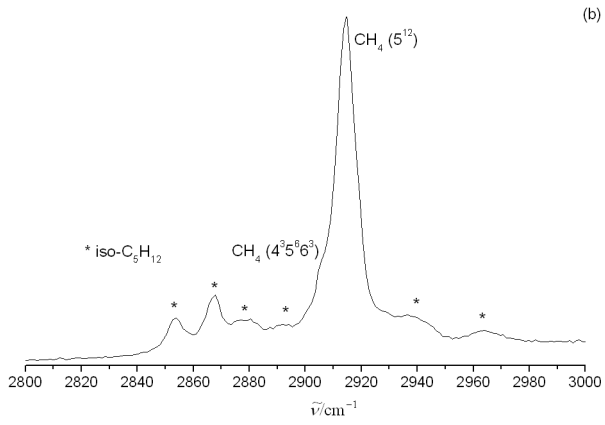


FIGURE 9. Raman spectra of gas hydrate crystals grown from a gas mixture containing 1% iso-C₅H₁₂ and 99% CH₄.





Tables:**TABLE 1.** Composition of gas mixtures.

Gas mixture	Name
2% C ₃ H ₈ 98% CH ₄	GM_C3
2% iso-C ₄ H ₁₀ 98% CH ₄	GM_isoC4
2% n-C ₄ H ₁₀ 98% CH ₄	GM_nC4
2% neo-C ₅ H ₁₂ 98% CH ₄	GM_neoC5
1% iso-C ₅ H ₁₂ 99% CH ₄	GM_isoC5

TABLE 1. van der Waals diameter of structure II hydrate formers.

Large hydrocarbon guest molecule	Guest molecule diameter/ppm
C ₃ H ₈	657
iso-C ₄ H ₁₀	657
n-C ₄ H ₁₀	786 (trans conformer)
	743 (gauche conformer)
	733 (cis conformer)
neo-C ₅ H ₁₂	658

TABLE 3. p, T conditions of time-dependent XRD experiments.

Gas mixture	T/K	p/MPa
GM_C3	267	1.26
GM_isoC4	267	0.93
GM_nC4	267	2.36
GM_neoC5	267	0.54

TABLE 4. Formation rate constants and Avrami exponents obtained for enclathration-controlled reaction step.

Gas mixture	k/min^{-1}	$k_{\text{error}}/\text{min}^{-1}$	n	n_{error}
GM_C3	2.04E-02	5.73E-03	0.86	0.07
GM_iso-C4	1.49E-02	5.84E-03	0.78	0.07
GM_n-C4	3.02E-02	2.44E-03	0.57	0.01
GM_neo-C5	5.69E-04	1.87E-04	1.71	0.07

TABLE 5. Formation rate constants obtained for diffusion-controlled reaction step.

Gas mixture	k/min^{-1}	$k_{\text{error}}/\text{min}^{-1}$
GM_C3	1.95E-04	3.15E-05
GM_iso-C4	-	-
GM_n-C4	-	-
GM_neo-C5	4.57E-05	1.76E-05